Rotational excitation of N_2 and Cl_2 molecules by electron impact in the energy range 0.01–1000 eV: Investigation of excitation mechanisms

Holger Kutz and Hans-Dieter Meyer
Theoretische Chemie, Physikalisch-Chemisches Institut, Universität Heidelberg, Im Neuenheimer Feld 253, D-69120 Heidelberg, Germany
(Received 20 September 1994)

The rotational excitation of N_2 and Cl_2 molecules on electron impact is investigated over a wide range of incident electron energies (0.01–1000 eV). Two different excitation mechanisms are reported, the importance of which depends on the impact energy. At low electron energies only a few rotational quanta are exchanged, and the differential cross section decreases exponentially with Δj. At high electron energies the excitation spectrum shows a rotational rainbow, i.e., the differential cross section has a maximum at a relatively high Δj. The location of this maximum depends on electron energy E and scattering angle θ. For intermediate energies there is an interplay of these two mechanisms. It can be seen that the contributions of both mechanisms can roughly be added to yield the cross section for the observed process.

PACS number(s): 34.80.Gs

I. INTRODUCTION

Scattering processes include electronic, vibrational, or rotational excitation of the target. Because of the very low energy transfer the latter was difficult to observe, but, due to improving experimental techniques, the interest of experimentalists and theorists has been growing during the last two decades. Some 15 years ago it was observed in heavy-particle scattering systems that large rotational quantum changes can occur in a single scattering event. This phenomenon was theoretically recognized as a rotational rainbow (see, e.g., [1–3]). These rotational rainbows were subsequently found in many other collision systems (see, e.g., [4–6]). It was widely believed that the dominance of a repulsive interaction was a necessary condition for these occurrences. In 1987 the surprising observation of a rotational rainbow in an electron-Na_2 cross beam experiment by Ziegler *et al.* [7,8] proved that this is not so. The experimental results were confirmed by calculations with different theoretical methods [9,10], and the rotational rainbow was interpreted as a consequence of the strong anisotropy of the potential (for a comprehensive review on rotational rainbows, see [11] and references therein).

Rotational rainbows in electron-molecule scattering for a couple of other targets have meanwhile been observed. In fact, today we know that this feature can be found in any electron-molecule system if the scattering energy and the scattering angle are large enough.

In this paper we will show that rotational rainbows are a specific high-energy (rotational) excitation mechanism, whereas at low energies a different mechanism dominates (which will be called the "normal" excitation mechanism). This is a quite useful division because the high- and low-energy spectra of the rotational excitation cross sections are very different from each other. Our interest was first directed towards the dominance of one or the other of these mechanisms for a given scattering energy and angle and then particular emphasis was given to the threshold of the rotational rainbow mechanism since we wanted to investigate if and how these mechanisms interacted with one another.

Two homonuclear molecules N_2 and Cl_2 were chosen as targets (these two molecules differ greatly in their internuclear distances and their polarizabilities) and the excitation cross sections were calculated for a wide variety of energies and scattering angles. Simultaneously, both scattering systems were investigated by an experimental group at the University of Kaiserslautern, Germany [12]. The good agreement between their and our data demonstrated the validity of our results. Furthermore, a large amount of theoretical and experimental data are available for N_2 which we could also compare with our results. The scattering system e^--Cl_2, on the other hand, has been studied neither experimentally nor theoretically before.

For the present calculations the well-known close-coupling ansatz was chosen. Local model potentials are adopted, and an improved version of the local exchange potential is introduced. All this is described in Sec. II. The various cross sections used are briefly defined in Sec. III. In Sec. IV the two scattering mechanisms are outlined in some more detail. In Sec. V our findings are interpreted and some interesting aspects are presented about the total cross sections. A short summary in Sec. VI concludes this paper.

II. MODEL POTENTIALS

A. The effective potential $V(\vec{r}, E)$

The Schrödinger equation was solved by the well-known close-coupling ansatz, i.e., it was treated as a partial differential equation, and transformed to a set of ordinary differential equations by expanding the wave

function, Schrödinger operator, and potential into partial waves. Then a close-coupling calculation was performed subject to the scattering boundary conditions. The whole procedure is described in detail elsewhere (see, e.g., [13,14]).

In order to avoid the Schrödinger equation becoming an integro-differential equation it is necessary to approximate the nonlocal potential by an effective local potential. Therefore the interaction potential is approximated by the sum of a static, an exchange, a correlation, and a polarization potential. All those parts can be calculated from the local charge density derived from a self-consistent-field (SCF) calculation of the neutral undisturbed target in its ground state. The static potential $V_{\rm st}(\vec{r})$ [15] is purely local and need not be approximated, whereas the exchange is approximated by an energy dependent local model exchange potential $V_{\rm ex}(\vec{r},E)$. Correlation and polarization are treated together to give an (energy independent) model correlation-polarization potential $V_{\rm copo}(\vec{r})$. The sum of these three expressions represents the effective potential

$$V(\vec{r},E) = V_{\rm st}(\vec{r}) + V_{\rm ex}(\vec{r},E) + V_{\rm copo}(\vec{r}). \tag{1}$$

This is the model potential used in the calculations discussed below. Next the model correlation-polarization and the model exchange potential are discussed in more detail.

B. Local model correlation-polarization potential

In order to obtain an expression for a model correlation-polarization potential we adopted an idea of O'Connell and Lane [16]. The local correlation potential $V_{\rm corr}$ is based on the free-electron-gas correlation energy which is a function of the charge density $\rho(\vec{r})$ alone. In the literature different expressions for this correlation energy are available [16–20]. In the present work we employed the same parametrization as Morrison and Saha [20].

As described by O'Connell and Lane [16] and Morrison and Saha [20] the polarization potential is approximated by its asymptotic form

$$V_{\rm pol}(r,\theta) = -\frac{\alpha_0}{2r^4} - \frac{\alpha_2}{2r^4}P_2(\cos\theta)\ . \tag{2}$$

Next the correlation potential is expanded into spherical harmonics and the innermost crossing point of the expansion coefficients $V_{\rm corr}(r,\lambda)$ and $V_{\rm pol}(r,\lambda)$ for $\lambda = 0,2$ is determined. For r larger than this crossing point one takes $V_{\rm pol}$ to represent the model correlation-polarization potential $V_{\rm copo}$ whereas for r smaller than the crossing point one takes $V_{\rm corr}$. All terms of the correlation potential with $\lambda > 2$ have been neglected. We have checked that this neglect changes the computed cross sections only marginally.

C. Local model exchange potential

The exchange potential based on the free-electron-gas model is used. It was first introduced by Slater [21–23] and then adopted by several authors (e.g., [15,16,24–29]).

The local model exchange potential is given by

$$V_{\rm ex}(\vec{r}) = -\frac{2}{\pi}K_F(\vec{r})F(\eta(\vec{r}))\ , \tag{3}$$

where the functions $K_F(\vec{r})$, $F(\eta)$, and $\eta(\vec{r})$ have the forms

$$K_F(\vec{r}) = \left[3\pi^2\rho(\vec{r})\right]^{1/3}, \tag{4a}$$

$$F(\eta) = \frac{1}{2} + \frac{1-\eta^2}{4\eta}\ln\left|\frac{1+\eta}{1-\eta}\right|\ , \tag{4b}$$

and

$$\eta(\vec{r}) = \frac{\kappa(\vec{r})}{K_F(\vec{r})}\ , \tag{4c}$$

respectively. Here K_F denotes the Fermi momentum and ρ the charge density which is taken to be the SCF charge density.

For the local momentum of the scattered electron $\kappa(\vec{r})$ we find different expressions in the literature. Hara defines [30]

$$\kappa^2_{\rm Hara}(\vec{r}) = k^2 + K_F^2(\vec{r}) + 2I\ , \tag{5}$$

where k denotes the (asymptotic) momentum of the scattering electron and I denotes the ionization potential of the target. This ansatz fails when $\vec{r}$ becomes large because then $\kappa^2_{\rm Hara}$ approaches k^2+2I instead of the correct value k^2. For this reason other authors (e.g., [28,31]) dropped the $2I$ term from the equation and called the method *asymptotically adjusted* (AA):

$$\kappa^2_{\rm AA}(\vec{r}) = k^2 + K_F^2(\vec{r})\ . \tag{6}$$

This expression is correct for large values of $|\vec{r}|$, but it gives insufficient results for the exchange potential for small $|\vec{r}|$.

To combine the advantages of these two expressions we introduce a parameter g and define

$$\kappa^2_g(g,\vec{r}) := k^2 + K_F^2(\vec{r}) + \frac{(2-g)(2I)K_F^2(\vec{r})}{(2-g)K_F^2(\vec{r}) + 2Ig}\ , \tag{7}$$

where g is a real number between 0 and 2. Equation (7) reproduces the Hara and the AA ansatz for $g = 0$ and $g = 2$, respectively.

For intermediate values of g our ansatz has the correct properties for both small and large distances $|\vec{r}|$. At small distances the relation holds $K_F^2(\vec{r}) \gg 2I$, and therefore $\kappa_g(g,\vec{r}) \approx \kappa_{\rm Hara}(\vec{r})$, whereas for large distances $K_F(\vec{r}) \to 0$, which leads to $\kappa_g(g,\vec{r}) \approx \kappa_{\rm AA}(\vec{r})$ for $r \to \infty$.

The $^2\Pi_g$-shape resonance of the N_2 molecule near 2.4 eV was used as a very sensitive criterion to investigate the influence of g in more detail. Model potential calculations were performed with several values for g and compared to a calculation using a nonlocal *ab initio* potential. We found that the cross sections for $g \approx 1$ matched very well the calculation based on the *ab initio*

exchange. Hence all our calculations on N_2 and Cl_2 were carried out with $g = 1$.

A typical example of such a test is given in Fig. 1 where the eigenphase sum δ_{sum} versus the scattering energy E is shown. The full model potential was used. Using the same Gaussian basis as in [32] for the SCF calculation, $\rho(\vec{r})$ was determined, and $V_{\text{st}}(\vec{r})$, $V_{\text{ex}}(E,\vec{r})$, and $V_{\text{copo}}(\vec{r})$ were calculated, the last adopting the polarizabilities cited in [17]. The exchange potential was created three times in order to compare $g = 1$ with Hara's ($g = 0$) and the asymptotically adjusted ($g = 2$) ansatz. These results were compared to two calculations of Meyer [32], who used an "exact" nonlocal exchange potential and introduced correlation and polarization effects by an optical potential. This optical potential was derived by a two-particle-hole Tamm-Dancoff approximation (2ph-TDA) [33,34] (solid curve in Fig. 1) and by algebraic diagrammatic construction complete until third order perturbation theory [ADC(3)] [35,36] (long and short dashes in Fig. 1). One can give arguments that the 2ph-TDA is likely to yield optical potentials that are too attractive whereas ADC(3) is supposed to give a potential that is not attractive enough [32]. The calculation with $g = 1$ lies nicely between the two results which used an optical potential whereas the exchange derived with Hara's ansatz ($g = 0$) is not attractive enough (the resonance appears at too high energy). With the AA approach, on the other hand, the potential becomes so attractive that the resonance completely vanishes and turns into a bound state. This result shows that setting $g = 1$ is an improvement to the model exchange potential.

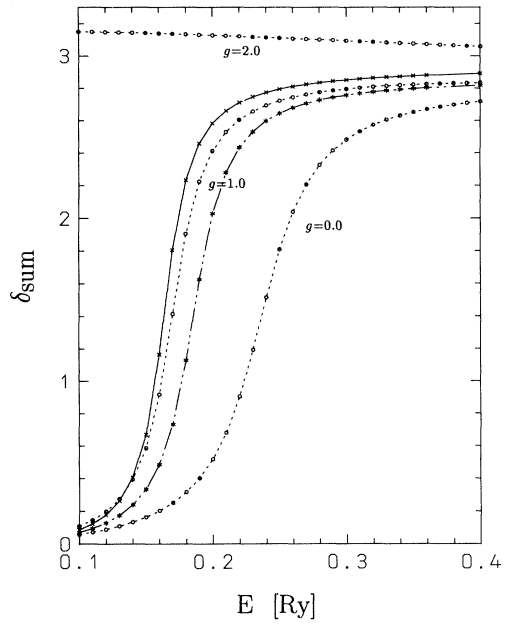

FIG. 1. e^--N_2 Π_g resonance: Eigenphase sums δ_{sum} versus scattering energy E. Comparison of scattering calculations with different parameters g in the model exchange potential (○, dashed curves, g=0.0,1.0,2.0) with two calculations of Meyer [32] employing two different optical potentials: 2ph-TDA (×, solid line) and ADC(3) (*, alternately dashed curve). The 2ph-TDA approximation is known to yield optical potentials that are too attractive, whereas optical potentials calculated with the ADC(3) approximation are likely to be not attractive enough.

Note that with the above comparison the quality of both the correlation-polarization potential and the exchange potential has been tested. Scattering calculations using the model exchange potential alone were also performed and compared with "exact" static-exchange results for N_2 and HF [14]. It was found that $g = 1$ was always a reasonable choice [37].

III. CALCULATION OF CROSS SECTIONS

Differential cross sections which depend on both the scattering angle θ and the rotational transition $\Delta j = j_f - j_i$ are of interest here, in particular those that refer to the rotational ground state $j_i = 0$. These differential cross sections are called "excitation cross sections" or "excitations" $\frac{d\sigma}{d\Omega}(j \leftarrow 0,\theta)$. The equations used for the evaluation of the excitation cross sections are given in [15,37,38]. Here we make some brief remarks only about the approximations and their range of applicability.

From the scattering calculation described in Sec. II the fixed nuclei S matrix is obtained. The nuclear motion is then included via the adiabatic nuclei approach [38]. This is a good approximation if the time of interaction between electron and target is short compared to characteristic times of a rotational period and if the energy transfer ΔE is small compared to the total energy E of the scattering electron. Both conditions are fulfilled down to energies of about 10^{-2} eV for both the N_2 and the Cl_2 molecule.

The target was treated as a rigid rotor; hence no vibrational excitations are taken into account. The cross sections for vibrational excitations are indeed very small (see, e.g., [39] for N_2), because due to the huge difference in mass between electron and target the direct excitation mechanism is very inefficient. However, in the vicinity of shape resonances vibrational excitation becomes very important, but the energy regions of resonances have been of minor interest here.

Due to the potential model adopted, electronic excitations were neglected also. It is known that N_2 can be electronically excited by electron impact above 10 eV [39] and Cl_2 above a few eV. The cross sections for electronic excitation are not always small compared to those of rotational excitation. The possibility of electronic excitation is assumed to be insignificant and will not alter the scattering going into the electronically elastic channel. The electronically inelastic flux may reduce somewhat the cross sections for electronically elastic scattering but the rotational distribution within the elastic channel will be almost unchanged. This assumption is supported by the rather good agreement between our computed cross sections and measured ones.

From the excitation cross section two more kinds of differential cross sections which are used in this paper can easily be derived. Summing over all final rotational states j yields the differential cross section

$$\frac{d\sigma}{d\Omega}(\theta) = \sum_{j=0}^{\infty} \frac{d\sigma(j \leftarrow 0\,,\,\theta)}{d\Omega}\,. \tag{8}$$

If we integrate the excitation cross section over all space we obtain the "integrated excitation"

$$\sigma(j \leftarrow 0) = \int \frac{d\sigma(j \leftarrow 0\,,\,\theta)}{d\Omega}\, d\Omega\,. \tag{9}$$

Note that the differential cross section and the integrated excitation were not evaluated by using their definitions [Eqs. (8) and (9)], but were calculated directly from the fixed nuclei S matrix. The relevant equations can be found in [37].

Of considerable interest is also the total cross section $\sigma_{\rm tot}$. For linear molecules where m is a good quantum number we may calculate $\sigma_{\rm tot}$ as sum of the partial cross sections $\sigma(m)$

$$\sigma_{\rm tot} = \sum_{m=0} \sigma(m). \tag{10}$$

The partial cross sections $\sigma(m)$ are related to the fixed nuclei S matrix via

$$\sigma(m) = \nu_m \frac{\pi}{k^2} \sum_{\ell,\ell'=0} \left| S^{(m)}_{\ell\ell'} - \delta_{\ell\ell'} \right|^2\,, \tag{11}$$

where ν_m denotes the symmetry degeneracy factor (ν_0=1, ν_m=2 for $m > 0$), $k = (2E)^{1/2}$ is the momentum of the incident electron, and $S^{(m)}_{\ell\ell'}$ is a shorthand notation for the S matrix $S_{\ell m \ell' m'}$, which is diagonal in m because we consider linear molecules.

Alternatively, we will write $\sigma(\Sigma)$ for $\sigma(m = 0)$, $\sigma(\Pi)$ for $\sigma(m = 1)$, etc. For homonuclear molecules one may split the partial cross sections further into a gerade and ungerade part, e.g., $\sigma(\Sigma_g)$. The gerade (ungerade) part is obtained by summing in Eq. (11) only over even (odd) ℓ, respectively.

IV. ROTATIONAL EXCITATION MECHANISMS

There are two different mechanisms for the rotational excitation depending on the energy of the scattering electron, the target, and the scattering angle θ. We will refer to one of them as the "normal" excitation or "low-energy excitation" and to the other as the "rotational rainbow" or "high-energy excitation."

At low incident energy the electron essentially interacts with the long range parts of the potential of the target. For homonuclear molecules these are the quadrupole potential and the polarization potential. The angular dependence of both these potentials is given by the second Legendre polynomial. If we further assume validity of the "distorted-wave Born" approximation [40] we find that only rotational transitions $\Delta j = 0$ and $\Delta j = 2$ appear in first order Born approximation, whereas $\Delta j = 4$ appears only in second order Born. The cross section falls off exponentially with increasing Δj and in most cases only the transitions $\Delta j = 0, 2$ carry non-negligible intensities.

For high electron energies it has been found (see, e.g., [7–9,11,41,42]) that excitation cross sections may be very large for high final rotational states j_f. This phenomenon has been identified as a rotational rainbow; it can be rationalized in the following way.

For the observation of a rotational rainbow not only high electron energy but high scattering angles are needed as well. The scattering angle can only be large when, classically speaking, the impact parameter is small, i.e., the scattering electron must penetrate the electron cloud and come near the core of the molecule. We may further simplify this picture and assume that the scattering electron "bounces off" one of the nuclei of the diatomic molecule while the other is a "spectator." This classical picture, which is called the spectator model [11], is depicted in Fig. 2. The momentum transfer of the electron changes the angular momentum of the target:

$$J = kR \sin\left(\frac{\theta}{2}\right) \sin\alpha\,. \tag{12}$$

It can be shown that a rotational rainbow arises for $\alpha = 90°$ [9,11,42] and

$$J_R = kR \sin\left(\frac{\theta}{2}\right)\,. \tag{13}$$

The (normalized) classical transition probability is given by (cf. [42], Eq. (40))

$$P(J \leftarrow 0, \theta) = \frac{2J}{J_R \sqrt{J_R^2 - J^2}}\,. \tag{14}$$

In quantum mechanics the following differences to the classical picture emerge:

(i) The spectrum is discrete;

(ii) the spectrum shows a maximum at a transition j_f which is somewhat lower than J_R, given by Eq. (13);

(iii) the oscillations in the classically allowed region ($j_f < J_R$) can be interpreted as interferences between different classical trajectories which lead to the same j_f; and

(iv) the cross sections in the classically forbidden region are not zero but decrease rapidly. The quantum

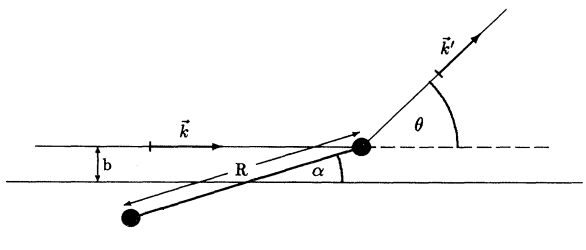

FIG. 2. Electron-molecule collision in the spectator model (classical picture). An electron with momentum $\vec{k}$ is scattered off one nucleus of a diatomic molecule while the other nucleus is the "spectator." R denotes the internuclear distance. The electron is scattered with angle θ and has momentum $\vec{k}'$ after collision. Because the energy transferred to the molecule at impact is small compared to the total energy of the scattering electron we may write $|\vec{k}'| \approx |\vec{k}| \equiv k$.

cross section within the spectator model is given by ([9], Eq. (5))

$$\frac{d\sigma}{d\Omega}(j \leftarrow 0, \theta) = C(2j+1) j_j^2(kR\sin(\theta/2)) \ , \qquad (15)$$

where the symbol $j_j(x)$ denotes the spherical Bessel function and C is a normalization constant.

V. RESULTS AND DISCUSSION

A. The total cross sections

We investigated the total cross sections of Cl_2 and N_2 in the energy range from 10^{-2} eV to 1000 eV and from 10^{-3} eV to 1000 eV, respectively. Brief comments on the basis sets used for the SCF calculations performed to derive the charge densities and on some other parameters for the model potentials are in order. These values were used for all calculations discussed in this paper.

For N_2 the basis of [43], Table 1 and Table 2 was used. The contraction scheme of [43], Table 3, No. 14 was slightly modified by contracting only the first two p functions and treating the remaining p functions as separate. From the charge density the model exchange potential was calculated with $g = 1$ and the ionization potential was set to I=1.146 Ry [28]. The polarizabilities needed for the model correlation-polarization potential were taken from [44], i.e., $\alpha_0 = 11.29$ a.u. and $\alpha_2 = 2.713$ a.u. The basis set for Cl_2 was taken from [45]. In the model exchange potential calculation again $g = 1$ but I=0.8452 Ry [46] was used and for the calculation of the model correlation-polarization potential the polarizabilities $\alpha_0 = 24.42$ a.u. and $\alpha_2 = 16.293$ a.u. were taken according to Ref. [44]. For the scattering calculation of both N_2 and Cl_2 up to 80 angular momentum terms ($\ell_{\max} = 158$) and up to 16 scattering symmetries ($m_{\max} = 7$) were used.

The calculated and measured [12] total cross sections of Cl_2 are shown in Fig. 3(a). Below 10 eV there is a surprisingly large difference (about two orders of magnitude) in the results obtained with the full model potential and a static-exchange (SE) calculation (where we simply omitted the model correlation-polarization potential). The curve obtained with the full model potential shows a deep minimum in about the same energy range where there is a maximum in the SE calculation, i.e., the scattering calculation is extremely sensitive to small alterations in the effective potential. By investigating the partial cross sections (for more details, cf. [47]) we found that the minimum in the full calculation is due to a minimum in Σ_g symmetry whereas the maximum in the SE calculation is caused by large cross sections in Σ_u symmetry.

Therefore the minimum in the "full" calculation is of the Ramsauer type. The peak in the SE calculation is more difficult to explain. In the neutral Cl_2 molecule the $5\Sigma_u$ orbital is the lowest unoccupied molecular orbital (LUMO). If the scattering electron occupies this orbital a weakly bound state is formed (the Cl_2^- ion is stable) when the full model potential is used. The SE potential, on the other hand, is less attractive and hence this state is no longer bound but becomes a shape resonance which is the cause of the observed maximum.

In a similar way the total cross sections of N_2 can be explained [Fig. 3(b)]. Let us first turn to the often investigated $^2\Pi_g$ shape resonance. Our calculation with the full model potential reproduces very well the correct position of this resonance at 2.4 eV, whereas in the SE calculation the position of the resonance is shifted to 4.3 eV.

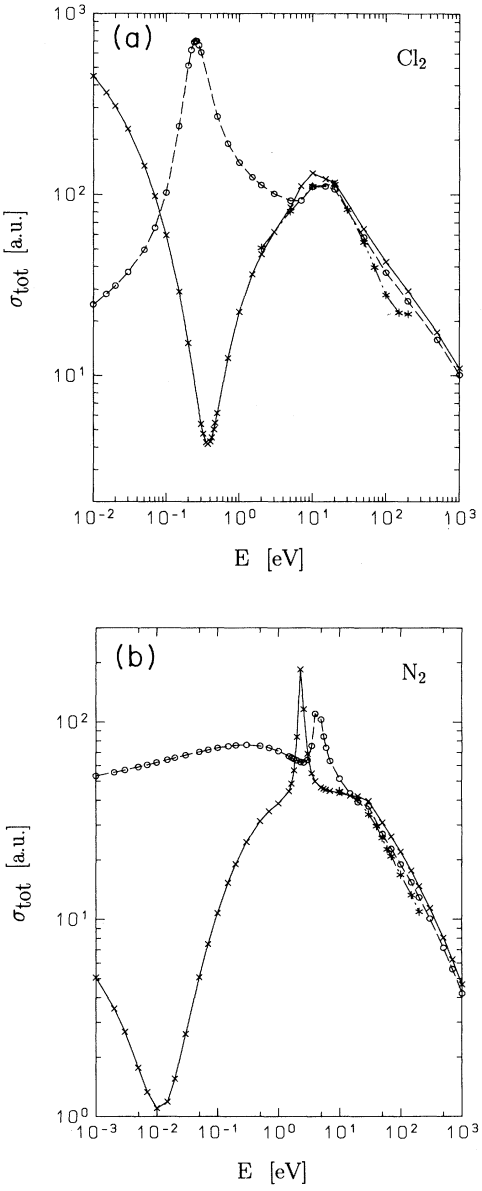

FIG. 3. Total cross sections σ_{tot} versus scattering energy E for (a) Cl_2 molecule and (b) N_2 molecule. We compare calculations performed with the full model potential ($\times$, solid line) with static + model exchange calculations ($\bigcirc$, long dashes). Experimental results of Gote [12] are shown as well ($*$, alternately dashed line).

This shift is due to the fact that the SE potential is less attractive.

As in the Cl_2 molecule a prominent Ramsauer minimum is found, which in this case is very deep and broad. Again there is no Ramsauer minimum in the calculation with the less attractive SE calculation. The relatively high cross sections in this area are dominated by the Σ_g symmetry.

For both molecules (Cl_2 and N_2) very similar results for both model potentials ("full" and SE) are obtained when the scattering energy is higher than about 10 eV.

Both molecules were experimentally investigated by Gote [12]. The total cross sections which were evaluated by numerical integration of his differential cross sections (extrapolated for small angles) are also shown in Figs. 3(a) and 3(b). Our calculations agree well with his results.

B. The differential cross sections

Differential cross sections of N_2 and Cl_2 for a great variety of scattering energies and scattering angles were calculated. At low energies the shape of the differential cross sections varies strongly with the scattering energy. At high scattering energies (from about 10 eV) the forward direction becomes more and more dominant, leading to large cross sections in the forward direction which decrease rapidly with the scattering angle θ.

We compared many of our results with experimental data. In all cases the correspondence was good or at least satisfactory. Figure 4 shows an example for each of the two molecules. In Fig. 4(a) we see a comparison between our calculation (full line) and two measurements. For the Cl_2 molecule there are no results in the literature apart from those of Gote [12]. In Fig. 4(b) cross sections at 2.0 eV are shown, the lowest measured energy and the one which agrees *worst*. The higher the energy the better the agreement, which becomes excellent above 10 eV.

C. The excitation cross sections

The main interest in this work was the investigation of rotational excitation of the molecules caused by electron impact. From the shape of the spectra one can distinguish the two excitation mechanisms discussed earlier. It turned out to be far more difficult to make statements about the intermediate energy range where both mechanisms contribute to the process. In the following these aspects will be discussed in more detail.

The excitation cross sections $\frac{d\sigma}{d\Omega}(j \leftarrow 0, \theta)$ versus the final rotational state j have been calculated for a large number of scattering energies and angles [47]. In the following we shall concentrate on calculations with the full model potential.

A first interesting observation can be made in the energy region of the Ramsauer minimum ($E \approx 10^{-2}$ eV for N_2, $E \approx 5 \times 10^{-1}$ eV for Cl_2), i.e., at energies low enough that a "normal" excitation mechanism is expected. This is indeed the case, but with the peculiarity that the cross section of the elastic channel almost vanishes. This means that in this energy range the $2 \leftarrow 0$ excitation is the most probable one and practically all collisions lead to rotational excitation. The Ramsauer minimum seems only to affect the $0 \leftarrow 0$ channel. The region in which the cross section of the $2 \leftarrow 0$ excitation is higher than the elastic channel is quite broad: from $\sim .5 \times 10^{-3}$ eV to $\sim 2 \times 10^{-2}$ eV for N_2 and from $\sim 2 \times 10^{-1}$ eV to ~ 1 eV for Cl_2 if in the latter case the backward direction is considered only [37,47].

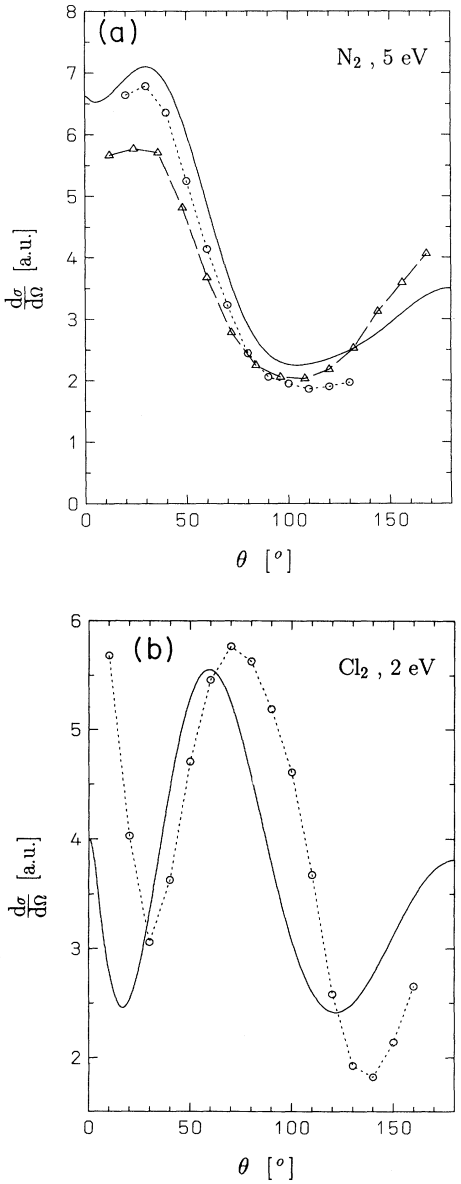

FIG. 4. Differential cross sections $\frac{d\sigma}{d\Omega}$ versus scattering angle θ. In (a) we compare our calculations (solid line) for the N_2 molecule and scattering energy E=5 eV with experimental results of Shyn and Carignan [48] (△, long dashed line) and of Brennan *et al.* [49] (○, short dashes). (b) shows cross sections for Cl_2 at E=2 eV. Our results (solid line) are compared to the measurements of Gote [12] (○, short dashes).

Next we will discuss the rotational rainbows at scattering angle θ=180°. At this angle the rotational rainbow can be observed best according to Eq. (13). Figures 5(a) and 5(b) show the result of our calculations. Because the differential cross section for θ=180° decreases rapidly with the scattering energies it was convenient to normalize the excitation cross sections such that the sum over all excitations for a given energy equals 1. For energies of 10–20 eV for N_2 and a few eV for Cl_2, respectively, the rotational rainbow begins to build. In Figs. 5(a) and 5(b) one can see how the maximum of the rainbow moves to higher j with increasing energy. The higher the energy the better the structure of the oscillations can be observed. At the same time the height of the maximum decreases because a higher percentage of collisions lead to other excitations. Note that the highest maximum for the Cl_2 molecule lies at higher values of j [Fig. 5(b)] compared to N_2 [Fig. 5(a)] (for same electron energy), which is simply due to the larger internuclear distance [cf., Eq. (13)].

In Figs. 6(a) and 6(b) the calculated spectra at 200 eV and 160° for (a) N_2 and (b) Cl_2 are compared with the experimental results of Gote [12] and the spectator model [cf. Eq. (15)]. The latter is a good description of the scattering process since the rainbow excitation mechanism applies at this scattering energy and angle. The normalization constant C of the spectator model was fixed by a least square fit relative to our calculation. The overall agreement between all three curves is very good apart from two values. In Fig. 6(a) the spectator model overestimates the $2 \leftarrow 0$ transition. In Fig. 6(b) the experimental $10 \leftarrow 0$ cross section is higher than both our calculation and the spectator model. A similar comparison with the experiment and (when appropriate) the spectator model was made for the majority of our excitation calculations. In almost all cases the agreement of the results was very good.

D. The integrated excitation

To reduce the amount of data substantially the excitations were integrated over space angle Ω [cf. Eq. (9)].

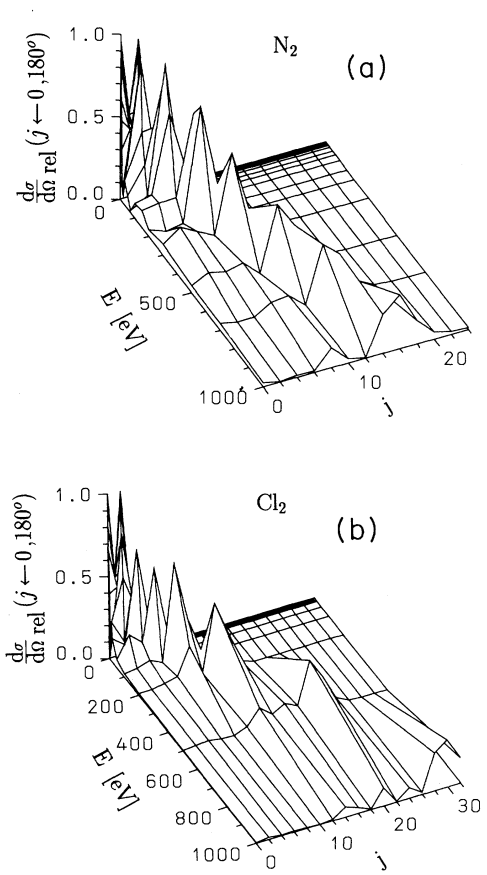

FIG. 5. Three-dimensional (3D) plot of the relative excitation cross sections $\frac{d\sigma}{d\Omega}_{\rm rel}(j \leftarrow 0, \theta = 180°)$ (cross sections were normalized to 1 for every scattering energy) versus rotational transition j and energy of the scattered electron E (eV) for N_2 (a) and Cl_2 (b). The calculations were made for fixed scattering angle $\theta = 180°$.

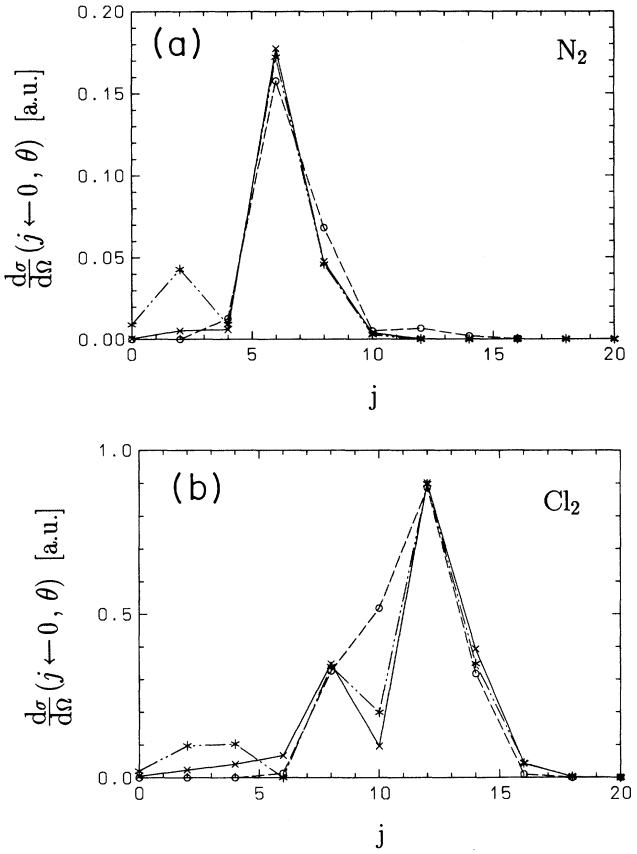

FIG. 6. Excitation cross sections $\frac{d\sigma}{d\Omega}(j \leftarrow 0, \theta)$ versus final rotational state j for (a) N_2 molecule and (b) Cl_2 molecule. The scattering energy and angle for both molecules were E=200 eV and θ=160°. We compare our calculations (×, solid line) with the experimental results of Gote [12] (○, long dashes) and the spectator model (*, alternately dashed curve).

Hence the rotational state of the molecule after the collision is selected for a given scattering energy disregarding the fate of the scattered electron.

If cross sections of the integrated excitations are plotted versus j one observes that the typical shape of the rotational rainbow has completely vanished even for very high scattering energies. The position of the minima and maxima of the oscillation structure depends on the scattering angle θ [cf. Eq. (13)]. Integration over this angle averages out these maxima and minima.

More information can be gained by plotting the integrated excitation cross section versus scattering energy for particular excitation channels. For the first four channels this is shown on Fig. 7. For the N_2 molecule [Fig. 7(a)] one observes that in the region of the Ramsauer minimum the $2 \leftarrow 0$ excitation cross section "overtakes" the elastic channel. This effect has been discussed earlier in this paper (cf. Sec. V C).

In the region where the rotational rainbow occurs the higher excitation channels gain some intensity compared to the region where the low-energy excitation mechanism dominates. This effect starts at a scattering energy of about 20 eV for N_2 [Fig. 7(a)] and at about 5 eV for Cl_2 [Fig. 7(b)]. In both cases it can be seen that the integrated cross section decreases with the final rotational state j.

E. Rotational excitations at fixed parameter J_R

According to the spectator model the shape of an excitation spectrum [cf. Eq. (15)] depends only on the value of J_R, which is defined in Eq. (13). Two series of calculations have been performed for each of the molecules N_2 and Cl_2. For each series the momentum k of the scattering electron and the scattering angle θ was varied such that the resulting J_R was kept constant. The corresponding spectrum was normalized to 1 and compared with the spectator model, which predicts identical spectra for the pure rainbow mechanism.

In Fig. 8 all calculated spectra were compared with the spectator model for N_2 and J_R=4.69 (a) and for Cl_2 and J_R=3.95 (b). Figure 8(a) shows that all curves correspond quite well with the result of the spectator model with the exception of scattering energy 70 eV and angle 180°. Further analysis of the data shows that the correspondence between the calculated spectrum and the spectator model improves for higher scattering energies.

This is also the case with the spectra of Fig. 8(b). Here the differences are even more obvious. The $2 \leftarrow 0$ peak of the 50 eV spectrum is much lower than the peak of the spectator model. Furthermore, a slight maximum at the excitation $6 \leftarrow 0$ appears which is not in the spectrum of the spectator model. In the 15 eV spectrum the position of the maximum has shifted to a higher excitation (i.e., $4 \leftarrow 0$). We could show that a better agreement with the spectator model could be obtained when a higher J_R parameter was used in the latter.

The other two series studied (i.e., J_R=9.72 for N_2 and J_R=7.20 for Cl_2) showed results which could be interpreted in exactly the same manner. The differences with the spectator model were smaller, though, because at higher J_R the rainbow scattering dominates the excitation mechanism more and more.

Our findings can be summarized in the following two statements.

(i) The spectra calculated for high scattering energies and low scattering angles agree better with the spectator model than those for low scattering energies and high scattering angles.

(ii) The excitations at lower scattering energies can be interpreted by the spectator model if one artificially

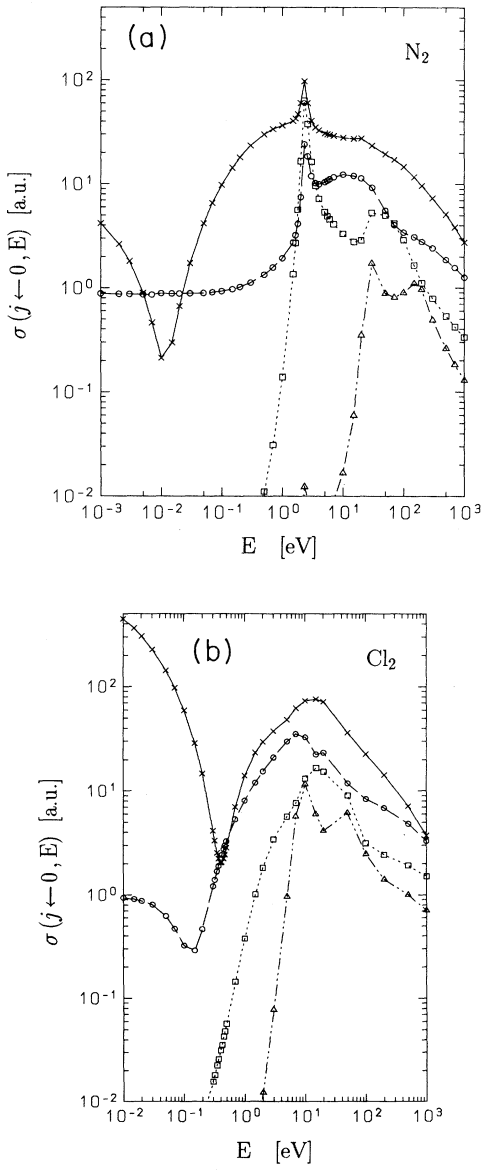

FIG. 7. Integrated excitation cross section $\sigma(j \leftarrow 0, E)$ versus scattering energy E for (a) N_2 molecule and (b) Cl_2 molecule. The following rotational excitation channels were considered: $0 \leftarrow 0$ (×, solid line), $2 \leftarrow 0$ (○, long dashes), $4 \leftarrow 0$ (□, short dashes), and $6 \leftarrow 0$ (△, alternately dashed line).

introduces a higher value for J_R.

There may be two explanations for this.

(1) The scattering electron is accelerated before impact by the attractive potential of the target. The impact (and the rotational excitation) therefore takes place at higher kinetic energy (i.e., higher J_R). After the impact the scattering electron is slowed down again by the potential. The energy of this process is taken from the overall potential (not from a distinct scattering channel). The higher the energy of the scattering electron before impact, the lower is the importance of this mechanism.

(2) The observed scattering angle is higher than predicted by the spectator model because the long range part of the potential further deflects the electron. This may lead to higher J_R. The importance of this effect increases the lower the scattering energy.

Both arguments explain the observed facts satisfactorily and allow a somewhat more detailed insight into the scattering process.

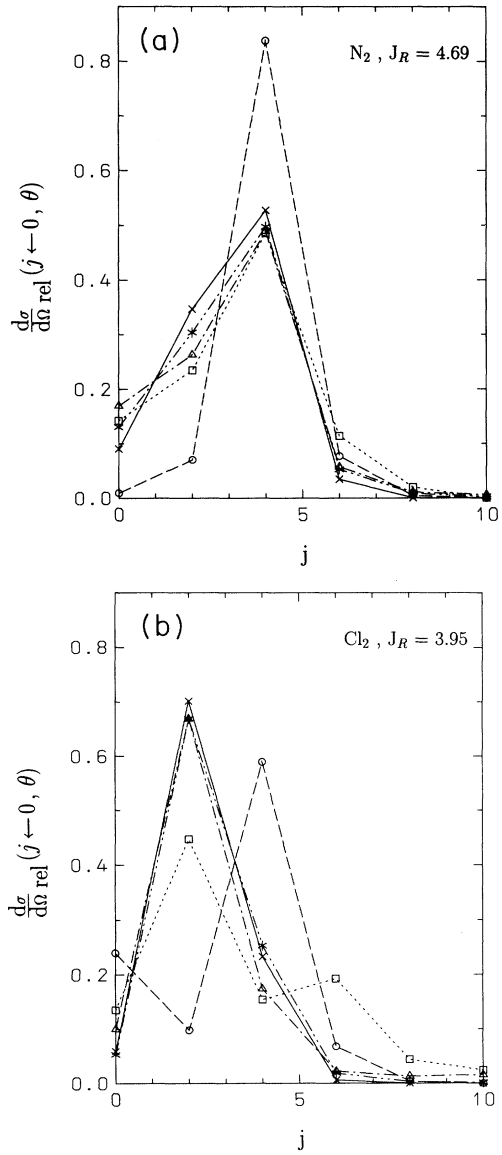

FIG. 8. Relative excitation cross sections $\frac{d\sigma}{d\Omega}_{rel}(j \leftarrow 0, \theta)$, versus rotational transition j while parameter J_R was held constant (cf. text). (a) For the N_2 molecule we compare the following pairs of scattering energies (scattering angles) (J_R=4.69): 70 eV (180.0°) (○, long dashes), 150 eV (86.1°) (□ , short dashes), 300 eV (57.5°) (△, alternately dashed line [long,short,...]), and 700 eV (36.8°) [*, alternately dashed line (long,short,short,...)]. (b) For the Cl_2 molecule the following pairs of scattering energies (scattering angles) were chosen (J_R=3.95): 15 eV (180.0°) (○, long dashes), 50 eV (66.4°) (□, short dashes), 100 eV (45.5°) [△, alternately dashed line (long,short,...)], and 500 eV (19.9°) [*, alternately dashed line (long,short,short,...)]. The graphs in both figures were compared to the spectator model of Korsch [42] which is represented by (×) and a solid line. All cross sections were normalized to 1.

F. Relative energy transfer

The investigation of the amount of energy which is transferred from the scattering electron to the target during the rotational excitation turned out to be a promising tool to characterize the excitation mechanism. To this end the excitation cross sections $\frac{d\sigma}{d\Omega}(j \leftarrow 0, \theta, E)$ are averaged leading to a considerable reduction of data. This is another advantage of this method. The energy ΔE which is transferred on average at a single scattering event is given by

$$\Delta E = B_e \frac{1}{\sum_j \frac{d\sigma}{d\Omega}(j \leftarrow 0, \theta, E)} \times \left(\sum_j \frac{d\sigma}{d\Omega}(j \leftarrow 0, \theta, E) j(j+1) \right) , \qquad (16)$$

where j denotes the final rotational state and B_e is the rotational constant which has the value $B_e = 3.025 \times 10^{-5}$ eV in the case of Cl_2 and $B_e = 2.4775 \times 10^{-4}$ eV for the N_2 molecule [46]. ΔE was divided by the energy E of the incident electron to arrive at the fraction of energy which is transferred to the molecule. This variable still depends on scattering energy and angle.

The relative energy transfer $\Delta E/E$ was plotted as a function of E for several scattering angles θ. Compared to the spectator model, which is, as mentioned before, only valid for the rotational rainbow scattering mechanism, the differences can be interpreted in favor of the low-energy scattering mechanism. Figure 9 shows our results in a doubly logarithmic scale for $\theta = 180°$.

Figure 9(a) depicts $\Delta E/E$ for the N_2 molecule. The spectator model (solid line) shows two completely different regions. At low scattering energy (up to about 10–20 eV) the relative energy transfer increases strongly. At the high-energy side a plateau is reached, i.e., the data oscillate about a constant value. These oscillations become flatter and more and more frequent. The low-energy side must be interpreted as a decrease of the effectiveness of the spectator model mechanism with decreasing energy. The plateau at high scattering energies can be understood in the following way. ΔE is an average

with weight factor $j(j+1)$ [Eq. (16)]. Thus $\Delta E \propto j^2$. If one assumes that most of the transferred energy will excite the rainbow channel J_R, and since $J_R \propto k$ [Eq. (13)], one can conclude that $\Delta E \propto E$ and $\Delta E/E \approx$ const. The oscillatory structure is due to the quantization of the angular momentum. Whenever the scattering energy, is such that the value of J_R is near an even integer the rotational rainbow peak is very distinct and the energy transfer is maximal. The opposite is the case when J_R is between two allowed rotational peaks. As $J_R \propto \sqrt{E}$ the oscillations become closer on a logarithmic energy scale with increasing energy. The higher the scattering energy, the more rotational excitation channels are open and the oscillations flatten towards the classical constant value.

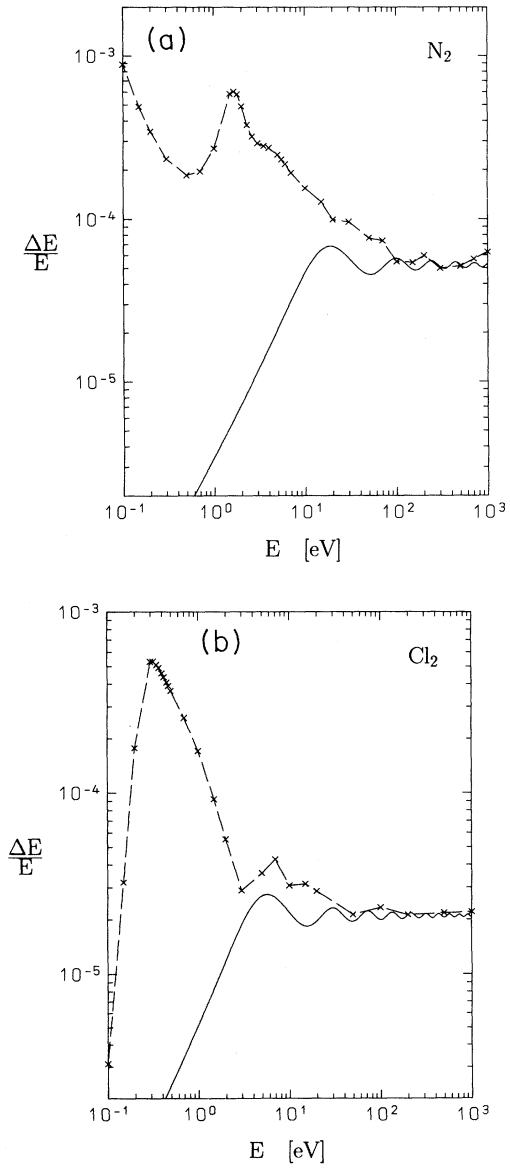

FIG. 9. Relative energy transfer $\Delta E/E$ versus scattering energy E at $\theta = 180°$ for (a) the N_2 molecule and (b) the Cl_2 molecule. Our calculations ($\times$, dashed line) are compared to the corresponding results of the spectator model (solid line).

Next the calculated spectrum (dashed line; the explicitly calculated energy points are marked with crosses) is compared to the spectator model. At low scattering energy (below 10 eV) rotational excitation can occur exclusively via the "normal" excitation mechanism, while excitation by the rotational rainbow mechanism leads to energy transfers which are several orders of magnitude lower than the "normal" ones. The $^2\Pi_g$ resonance appears as a peak of high energy transfer. At still lower energies the relative energy transfer reaches a minimum and then increases again. This effect will be discussed later in the Cl_2 spectrum. Between 10 eV and approximately 50 eV there is an intermediate range where both mechanisms take part in the excitation process simultaneously. As the calculated energy transfer is larger than the one of the spectator model we assume the two excitation mechanisms to be additive. At high scattering energy (in this case over 50 eV) the rainbow mechanism clearly dominates. The oscillations could not be reproduced by our calculation, which is, of course, due to the lack of sufficiently dense energy points. With the last two scattering energies the relative energy transfer appears to become higher. This is likely to be caused by the lack of convergence of our calculation because at very high energies it is necessary to take more scattering symmetries into account.

In Fig. 9(b) the results based on the spectator model for the Cl_2 molecule show exactly the same features as already discussed for N_2. Because of the longer internuclear distance the region of the rotational rainbow starts at lower energy. At energies below ≈ 3 eV only the low-energy mechanism is responsible for excitation. The intermediate region where both mechanisms contribute extends from about 3 eV to approximately 20 eV. Above this energy the rotational rainbow mechanism dominates. At 0.3 eV a very sharp maximum is seen. This coincides with the energy of the Ramsauer minimum [cf. Fig. 3(a)]. At first glance it might be surprising that a minimum in the cross section leads to a maximum in the relative energy transfer. But if one recalls Fig. 7(b) it immediately becomes evident that the $2 \leftarrow 0$ excitation channel dominates the elastic one, which leads to a disproportional energy transfer (cf. the discussion of Sec. V D).

Comparisons of our calculations with the spectator model for other scattering angles showed very similar results, except that then the rainbow mechanism — as expected — takes over at somewhat higher scattering energies. Investigating the relative energy transfer turned out to be a very convenient method to study the interplay of the discussed excitation mechanisms in more detail.

VI. CONCLUSION

We have investigated the electron scattering from N_2 and Cl_2 molecules with special emphasis on rotational excitation.

The scattering process was described by performing close-coupling calculations. Local model potentials have

been used to account for exchange, correlation, and polarization effects. We could improve the model exchange potential somewhat by introducing a parameter g which was later set to $g = 1$. Nuclear dynamics has been included in the adiabatic nuclei approximation. Moreover the molecule was treated as a rigid rotor. With these approximations some limitations were introduced. The scattering event has to be fast compared to typical times for rotational motion, the energy transferred to the target has to be small compared to the kinetic energy of the scattering electron, and finally vibrational and electronic excitations were excluded (the latter due to the potential model). However, only the exclusion of electronic excitation may be a questionable approximation. As discussed in Sec. III, one has reasons to believe that the existence of open channels for electronically inelastic scattering has only a negligible effect on the rotational distributions for electronically elastic scattering.

The very prominent feature in the spectrum of the total cross section for N_2 is the $^2\Pi_g$ resonance peak at 2.4 eV. This peak is shifted to ≈ 4 eV if we omit correlation and polarization effects, i.e., use the less attractive SE potential. The total cross sections of N_2 and Cl_2 both show a very deep and broad Ramsauer minimum at lower scattering energy. These minima are extremely sensitive to small changes of the potential and vanish completely when the SE potential is used. In the Cl_2 spectrum a maximum appears at almost the same position due to an (artificial) Σ_u shape resonance.

Two rotational excitation mechanisms have been studied. At low scattering angles and energies only a few rotational quanta are transferred ("normal" excitation mechanism) whereas in the case of high angles and energies many rotational quanta can be exchanged, i.e., the rotational rainbow mechanism applies. If the excitation cross sections are plotted versus rotational excitation Δj for a given scattering energy and angle both mechanisms can be distinguished by the typical shape of the spectra. On the other hand, little information can be gained in this way on the intermediate region where both mechanisms are active.

An interesting observation could be made concerning rotational excitation at scattering energies in the range of the Ramsauer minimum: a minimum is shown in the rotationally elastic channel indicating that almost every scattering event leads to an excitation $2 \leftarrow 0$.

As discussed the spectra of rotational rainbows can be described quite well by the so called "spectator model." In this model the shape of the spectrum (in the case of a diatomic molecule) only depends on $J_R = kR\sin(\theta/2)$ where R denotes the internuclear distance and k the momentum of the incident electron and the scattering angle θ. Several series of scattering calculations with fixed J_R (by choosing appropriate energy-angle pairs) were compared with this model, showing that the correspondence improved with higher incident energy. This was interpreted as long range effects by the scattering potential.

The relative energy transfer $\Delta E/E$ (energy transfer on average per scattering event divided by the total energy) was calculated for several scattering angles and many scattering energies and compared to the corresponding results for the spectator model. Three energy regions could be clearly distinguished. At low scattering energies excitation is only possible via the "normal" excitation mechanism (spectator model energy transfers are several orders of magnitude lower). In this region maxima in energy transfer are observed at energies around the Ramsauer minimum and at resonance energies. At the intermediate region both mechanisms additively contribute to the total energy transfer. At high scattering energies our calculations merge with the spectator model and excitation occurs via the rotational rainbow mechanism. The energy transfer plotted versus the scattering energy becomes constant except for small oscillations. This behavior could be explained satisfactorily.

Several results on the N_2 molecule have been compared to calculations or measurements in the literature. These, as well as comparison of our calculated cross sections for both scattering systems to the results of Gote, show good agreement.

ACKNOWLEDGMENTS

We thank Professor H. Ehrhardt and in particular Dr. M. Gote, Kaiserslautern, for valuable discussions and for providing us with their experimental results prior to publication. This work has been supported by Deutsche Forschungsgemeinschaft under SFB 91 "Energy Transfer in Atomic and Molecular Collisions."

[1] D. Beck, U. Ross, and W. Schepper, Z. Phys. A **290**, 131 (1979).
[2] J. R. Serri, A. Morales, W. Moskowitz, D. E. Pritchard, C. H. Becker, and J. L. Kinsey, J. Chem. Phys. **72**, 6304 (1980).
[3] K. Bergmann, U. Hefter, A. Mattheus, and J. Witt, Chem. Phys. Lett. **78**, 61 (1981).
[4] A. W. Kleyn, A. C. Luntz, and D. J. Auerbach, Phys. Rev. Lett. **47**, 1169 (1981).
[5] **R. Schinke, Chem. Phys. 85, 5049 (1986).**
[6] U. Hefter, P. L. Jones, A. Mattheus, J. Witt, K. Bergmann, and R. Schinke, Phys. Rev. Lett. **46**, 915 (1981).
[7] G. Ziegler, M. Rädle, O. Pütz, K. Jung, H. Ehrhardt, and K. Bergmann, Phys. Rev. Lett. **58**, 2642 (1987).
[8] G. Ziegler, S. V. K. Kumar, M. Rädle, K. Jung, H. Ehrhardt, K. Bergmann, and H.-D. Meyer, Z. Phys. D **16**, 207 (1990).
[9] H. J. Korsch, H. Kutz, and H.-D. Meyer, J. Phys. B **20**, L433 (1987).
[10] **H. Kutz, Diplom-thesis, University of Heidelberg, 1987.**
[11] H. J. Korsch and A. Ernesti, J. Phys. B **25**, 3565 (1992).
[12] M. Gote (private communications).
[13] H.-D. Meyer, Phys. Rev. A **34**, 1797 (1986).
[14] H. Kutz and H.-D. Meyer, J. Phys. B **23**, 829 (1990).
[15] N. F. Lane, Rev. Mod. Phys. **52**, 29 (1980).

[16] J. K. O'Connell and N. F. Lane, Phys. Rev. A **27**, 1893 (1983).
[17] N. T. Padial and D. W. Norcross, Phys. Rev. A **29**, 1742 (1984).
[18] W. J. Carr, Jr. and A. A. Maradudin, Phys. Rev. **133**, A371 (1964).
[19] W. J. Carr, Jr., R. A. Coldwell-Horsfall, and A. E. Fein, Phys. Rev. **124**, 747 (1961).
[20] M. A. Morrison and B. C. Saha, Phys. Rev. A **34**, 2786 (1986).
[21] J. C. Slater, Phys. Rev. **81**, 385 (1951).
[22] J. C. Slater, *Quantum Theory of Matter*, 2nd ed. (McGraw-Hill, New York, 1960), Chaps. 16 and 17.
[23] J. C. Slater, Phys. Rev. **92**, 528 (1953).
[24] W. Kohn and L. J. Sham, Phys. Rev. **140**, A1133 (1965).
[25] M. E. Riley and D. G. Truhlar, J. Chem. Phys. **65**, 792 (1976).
[26] B. N. Bransden, M. R. C. Mc Dowell, C. J. Nobel, and T. Scott, J. Phys. B **9**, 1301 (1976).
[27] M. A. Morrison, N. F. Lane, and L. A. Collins, Phys. Rev. A **15**, 2186 (1977).
[28] M. A. Morrison and L. A. Collins, Phys. Rev. A **17**, 918 (1978).
[29] D. G. Truhlar, *Chemical Applications of Atomic and Molecular Electrostatic Potentials*, edited by P. Politzer and D. G. Truhlar (Plenum, New York, 1981).
[30] S. Hara, J. Phys. Soc. Jpn. **22**, 710 (1967).
[31] S. Salvini and D. G. Thompson, J. Phys. B **14**, 3797 (1981).
[32] H.-D. Meyer, Phys. Rev. A **40**, 5605 (1989).
[33] L. S. Cederbaum and W. Domcke, Adv. Chem. Phys. **36**, 205 (1977).
[34] J. Schirmer and L. S. Cederbaum, J. Phys. B **11**, 1889 (1978).
[35] J. Schirmer, L. S. Cederbaum, and O. Walter, Phys. Rev. A **28**, 1287 (1982).
[36] W. von Niessen, J. Schirmer, and L. S. Cederbaum, Comput. Phys. Rep. **1**, 57 (1984).
[37] H. Kutz, Ph.D. thesis, University of Heidelberg, 1994.
[38] D. M. Chase, Phys. Rev. **104**, 838 (1956).
[39] Y. Itikawa, M. Hayashi, A. Ichimura, K. Onda, K. Sakimoto, K. Takayanagi, M. Nakamura, H. Nishimura, and T. Takayanagi, J. Phys. Chem. Ref. Data **15**, 985 (1986).
[40] J. R. Taylor, *Scattering Theory* (Wiley, New York, 1972).
[41] S. V. K. Kumar, G. Ziegler, H. J. Korsch, K. Bergmann, and H.-D. Meyer, Phys. Rev. A **44**, 268 (1991).
[42] H. J. Korsch, H.-D. Meyer, and C. P. Shukla, Z. Phys. D **15**, 227 (1990).
[43] C. Salez and A. Veillard, Theor. Chim. Acta **11**, 441 (1968).
[44] J. Oddershede and E. N. Svendsen, Chem. Phys. **64**, 359 (1982).
[45] H. Partridge, NASA Technical Memorandum No. 89449, 1987 (unpublished).
[46] K. P. Huber and G. Herzberg, *Constants of Diatomic Molecules* (Van Nostrand Reinhold Company, New York, 1979), Vol. 4.
[47] H. Kutz, Appendix to the dissertation [37] with numerous tables of cross sections which will be sent on request (Theoretische Chemie, Universität Heidelberg, INF 253, D-69120 Heidelberg).
[48] T. W. Shyn and G. R. Carignan, Phys. Rev. A **22**, 923 (1980).
[49] M. J. Brennan, D. T. Alle, P. Euripides, S. J. Buckman, and M. J. Brunger, J. Phys. B **25**, 2669 (1992).